RSC Advances

PAPER

View Article Online
View Journal | View Issue

Cite this: *RSC Adv.*, 2025, **15**, 35322

A thermo-electrochemical cell with a threaded graphite electrode towards low-grade heat recovery

Genghua Wang,[a] Shiwei Zhang,[b] Xiaotian Li,[b] Jili Zheng,[*b] Lixia Wang,[b] Xinyu Zhou[b] and Jun Zhang[*b]

Thermo-electrochemical cells (TECs) are a promising technology for converting low-grade thermal energy into electricity through redox reactions. Despite extensive research, TECs still face challenges in practical applications due to their complex assembly processes, susceptibility to leakage, limited electrode reaction area, and low efficiency. In this study, TECs featuring threaded graphite electrodes were constructed. Owing to the enhanced reaction area, high thermal conductivity, and excellent electrolyte sealing capability of the threaded graphite electrode configuration, the TECs demonstrate exceptional electrical output and long-term stability. Through systematic optimization of electrode materials, electrode spacing, and electrolyte composition, the Seebeck coefficient of the TECs reached 2.5 mV K^{-1}. Under a temperature difference of 20 K, the TECs achieved a maximum power output of 100 mW m^{-2}, representing a fourfold enhancement compared to the original cell. Furthermore, a TEC stack was developed based on optimized single-unit configurations. Comprehensive evaluation confirmed the stack's performance and operational stability, underscoring its significant potential for practical applications in low-grade thermal energy harvesting.

Received 22nd July 2025
Accepted 10th September 2025

DOI: 10.1039/d5ra05300e

rsc.li/rsc-advances

1 Introduction

Extensive consumption of fossil fuels has led to energy shortage and global warming. Low-grade heat (temperature < 130 °C) from industrial wastewater, geothermal activities and solar heating accounts for about 1/3 of the primary energy consumption.[1,2] Energy harvesting, converting low-grade heat into available energy, is a promising approach to increase energy utilization efficiency and reduce greenhouse gas emissions.[3] To this end, some devices, such as thermoelectric generators[4,5] and thermal regenerative ammonia cells,[6,7] have been developed for direct thermoelectric conversion in the past decades. However, the use of thermoelectric generators and thermal regenerative ammonia cells is not cost-effective, and thermoelectric materials are often toxic and not available at low temperatures.[8]

Thermo-electrochemical cells (TECs) are an attractive technology to convert low-grade heat into electricity through an electrochemical pathway owing to convenient large-scale deployability, simple design, low maintenance costs, and commercial availability.[9,10] Generally, TECs harvest thermal energy *via* the electrochemical Seebeck effect based on redox reactions in the electrolyte. The Seebeck coefficient of TECs is in the order of mV K^{-1}, much higher than that of a thermoelectric generator (μV K^{-1}).[11,12] Theoretically, the output of TECs is based on thermodynamic and kinetic features. The thermodynamics can be reflected by entropic change, which depends on the key components, including ion mobility and electrolyte composition, while the kinetics relies on the rate of redox reactions, namely, current density. Significantly, an advanced electrode is indispensable for realizing high performance TECs by improving thermodynamic and kinetic features.

To increase the energy efficiency of TECs, different electrode materials have been constructed, including graphite rod/plates,[13,14] graphene, carbon nanotubes, copper,[15–17] nickel and platinum.[18,19] Among them, carbon-based electrodes have attracted increasing attention due to the advantages of fast redox processes, high specific surface area, and high thermal and electrical conductivity. For example, Im *et al.*[20] reported a carbon nanotube aerogel as a porous electrode; the prepared electrode exhibited a power density of 6.6 W m^{-2} for a 51 °C inter-electrode temperature difference. Li *et al.*[21] synthesized an anisotropic holey graphene aerogel as an electrode; the TEC with the prepared electrode delivered a power density of 3.6 W m^{-2} and a Seebeck coefficient of 1.3 mV K^{-1}. With an improved Seebeck coefficient and power output, the thermal conductivity is usually ignored, but it should be noted that the thermal conductivity of porous electrodes, such as graphene aerogels, is

[a]*College of Energy and Power Engineering, Zhengzhou University of Light Industry, Zhengzhou 450002, China*

[b]*College of New Energy, Collaborative Innovation Center for New Energy Vehicle of Henan Province, Zhengzhou University of Light Industry, Zhengzhou 450002, China. E-mail: zhangjun@zzuli.edu.cn; Fax: +86-371-6362-4381; Tel: +86-371-6362-4381*

rather low due to high porosity and abundant pore structure, even though graphene itself has an excellent thermal conductivity. In addition, the use of adhesive and heat-conducting materials is necessary to ensure the intimate contact between the electrode and heat exchanger, considering the necessity of thermal management during the operation of TECs. The unsatisfactory thermal conductivity of adhesive materials will hinder heat transfer and result in a limited temperature difference between the anode and cathode.[22] The integration of TECs faces the challenge of electrolyte leakage due to complicated packaging issues. Therefore, to meet the requirements of scaling up and practical applications, it is urgent to develop a TEC with satisfactory electrical conductivity for heat transfer and improved surface area for reaction, as well as a rational packaging design to prevent the leakage of electrolyte.[23,24]

To address these issues, in this study, a TEC with a threaded graphite electrode was proposed. The threaded surface design can increase the effective area for redox reactions, and the excellent thermal conductivity of graphite benefits the heat transfer and the maintenance of the temperature difference. In addition, the threaded design is a reliable sealing strategy to prevent electrolyte leakage without the use of adhesive materials. The electrochemical features of threaded electrodes were characterized, and the performance of the TEC with threaded electrodes was evaluated. The performance of the TEC was optimized, including the electrode materials, electrode spacing, and electrolyte. Finally, the TEC stack was constructed based on the TEC unit, and the feasibility of the TEC stack was demonstrated.

2 Experimental

2.1 Chemicals

Potassium ferricyanide, potassium ferrocyanide, sodium sulfate, anhydrous ethanol, and acetone were purchased from Tianjin Guangfu Co., Ltd. Guanidine hydrochloride and sodium acetate were purchased from Shanghai Aladdin Reagent Co., Ltd. Graphite rods (99.9%) were purchased from Shanghai Carbon Factory. Copper and titanium rods are purchased from Hebei Ketai Metal Materials Company. More detailed information on these materials is provided in Table 1; the optical image of the electrode material is shown in Fig. 1. All chemical reagents were of analytical grade without the need for further purification before use.

Data acquisition instrument (Agilent 34972A), China Keysight Technologies Co., Ltd. Electrochemical workstation (CHI660E), Shanghai Chenhua Instrument Co., Ltd. DC power supply (MPS 305), Beijing Chex Electronic Technology Co., Ltd.

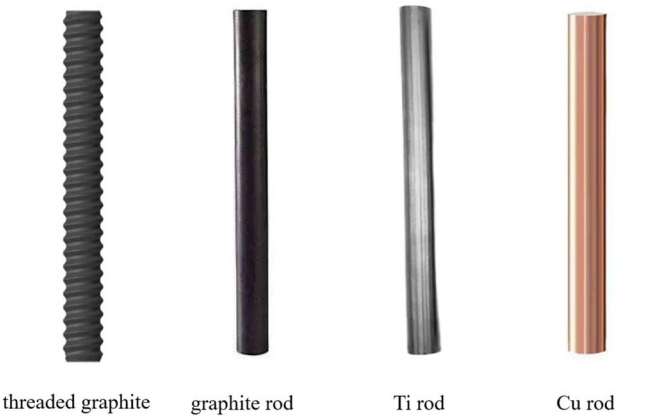

Fig. 1 Optical images of the threaded graphite electrode and graphite, Ti, and Cu rods.

2.2 Construction of the TEC system

A TEC was constructed based on threaded graphite electrodes. As shown in Fig. 2, a threaded graphite electrode (diameter 4 mm, length 60 mm) was fixed at both sides of the reactor with one end immersed in the electrolyte (15 mm). The cylindrical acrylic acid reactor was constructed with a diameter of 7 mm and a length of 20 mm; two sides of the reactor were designed with a threaded hole with a diameter of 4 mm for electrode fabrication. The electrolyte was prepared with 0.4 M $Fe(CN)_6^{4-}$/$Fe(CN)_6^{3-}$ solution.

2.3 Data analysis

To evaluate the thermopower of the TEC, the current and potential of the system were determined using an Agilent data acquisition instrument (34972A) with a time interval of 10 s. During the measurement, a hot bath was used as a heat source to maintain a constant temperature on the hot side of the TEC in the range of 30–70 °C. For the TEC, the Seebeck coefficient can be calculated based on the following equation:[22]

$$\mathrm{Se} = \frac{\Delta E}{\Delta T} \quad (1)$$

where ΔE is the open circuit voltage and ΔT is the temperature difference.

Table 1 Detailed information on materials such as threaded graphite, rods (graphite, Ti, Cu), and CNTs@threaded graphite

Materials	Thermal conductivity ($W\ m^{-1}\ K^{-1}$)	Resistivity ($\mu\Omega$ m)	Diameter (mm)	Length (mm)	Pitch (mm)	Density ($g\ cm^{-3}$)
Threaded graphite	115	9	10	300	1.5	1.82
Graphite rods	115	9	10	300	—	1.82
Ti rods	6.7	1.7	10	300	—	4.5
Cu rods	397	1.7×10^{-2}	10	300	—	8.45
CNTs@threaded graphite	300	5	5	100	1.5	1.82

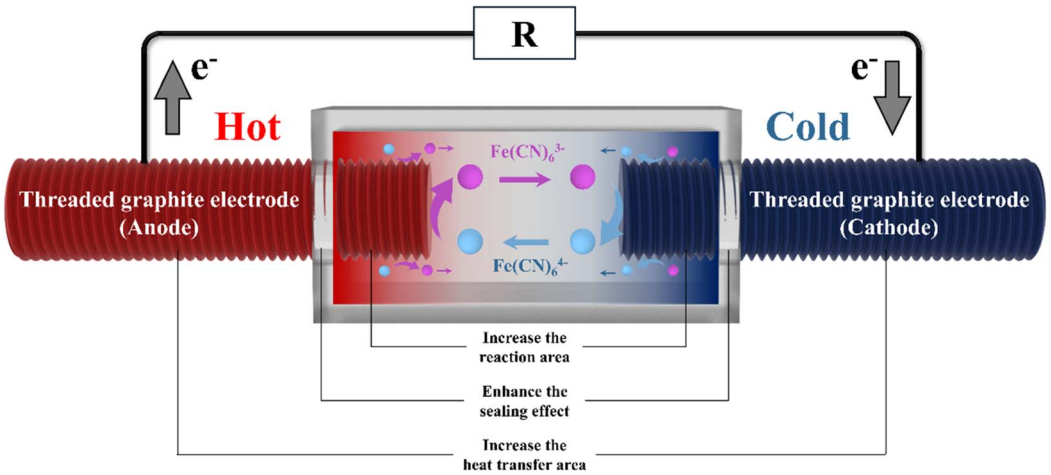

Fig. 2 Schematic of the thermochemical cell structure.

Energy conversion efficiency of the TECs is expressed as follows:[19]

$$\eta = \frac{(1/4)V_{OC} \times I_{SC}}{A_C \times k(\Delta T/d)} \quad (2)$$

where V_{OC} is the open circuit voltage, I_{SC} is the short circuit current, A_C is the cross-sectional area of the TEC, k is the thermal conductivity of the electrolyte, ΔT is the temperature difference, and d is the electrode spacing.

The energy conversion efficiency (η_r) relative to the Carnot heat engine efficiency is described as follows:

$$\eta_r = \frac{\eta}{(\Delta T/T_H)} \quad (3)$$

where η is the heat energy conversion efficiency and T_H is the temperature of the hot side of the TEC.

3 Results and discussion

3.1 Performance of TECs

3.1.1 The performance of a thermo-electrochemical cell with a single three-dimensional threaded electrode. During the continuous operation of a thermo-electrochemical cell, it is crucial to ensure that reaction products formed at one electrode can efficiently transport to the other electrode and participate in reactions. If neither electrode interface forms nor consumes the required redox molecules to generate electrons, the output of electrical energy cannot be sustained. The thermoelectromotive force in a thermo-electrochemical cell primarily originates from the free energy difference between reactants and products at the electrolyte–electrode interface, which is closely related to temperature. Therefore, the design of electrodes and the resulting temperature gradients directly affect the performance of thermochemical batteries.

As shown in Fig. 3, which investigates the influence of different graphite electrode structures on the performance of thermo-electrochemical cells, the performance of different electrodes was evaluated by short-circuit current, maximum output power, and open-circuit voltage under the same hot electrode temperature and projected area conditions. As shown in Fig. 3a and b, the short-circuit current density of the traditional flat-plate electrode is 1.35 A m^{-2}, that of the columnar electrode is 4.1 A m^{-2} (an increase of approximately 2.1 times), and that of the threaded rod electrode is further increased to 5.0 A m^{-2} (a 2.7-fold increase compared to the traditional electrode). Meanwhile, the thermochemical cell with a three-dimensional threaded rod electrode has the maximum output power of 25 mW m^{-2}, which is 2.6 times higher than that of the flat-plate electrode. The significant performance improvement of the threaded rod electrode thermochemical cell is mainly attributed to the design of the electrode structure. The three-dimensional threaded structure may increase the electroactive surface area available for redox reactions, thereby promoting the improvement of short-circuit current. In addition, for the three different electrode structures, the characteristics of the electrolyte solution are consistent, so their Seebeck coefficients should be the same. However, their open-circuit voltages differ: the columnar electrode and the threaded rod electrode are basically the same and significantly higher than the flat-plate electrode structure. This may be caused by different temperature differences between the electrodes, which is experimentally verified in subsequent sections.

For the performance of thermochemical batteries, in addition to the above evaluation indicators, efficiently generating usable electrical energy from temperature differences is crucial. Therefore, the area power density parameter $P_{max}/(\Delta T)^2$ derived from the temperature difference between electrodes is a key metric for measuring system performance. As shown in Fig. 3c, the corresponding $P_{max}/(\Delta T)^2$ values increased from 0.035 mW K^{-2} m^{-2} for the flat-plate electrode cell to 0.043 mW K^{-2} m^{-2} for the columnar cell and 0.066 mW K^{-2} m^{-2} for the threaded columnar cell. Compared with the flat-plate electrode cell, the $P_{max}/(\Delta T)^2$ of the threaded columnar cell is doubled.

The flat-plate cell limits the charge exchange of redox ions in the electrolyte, thereby degrading cell performance. In contrast, the columnar and threaded structures of three-dimensional columnar batteries significantly regulate the interfacial area

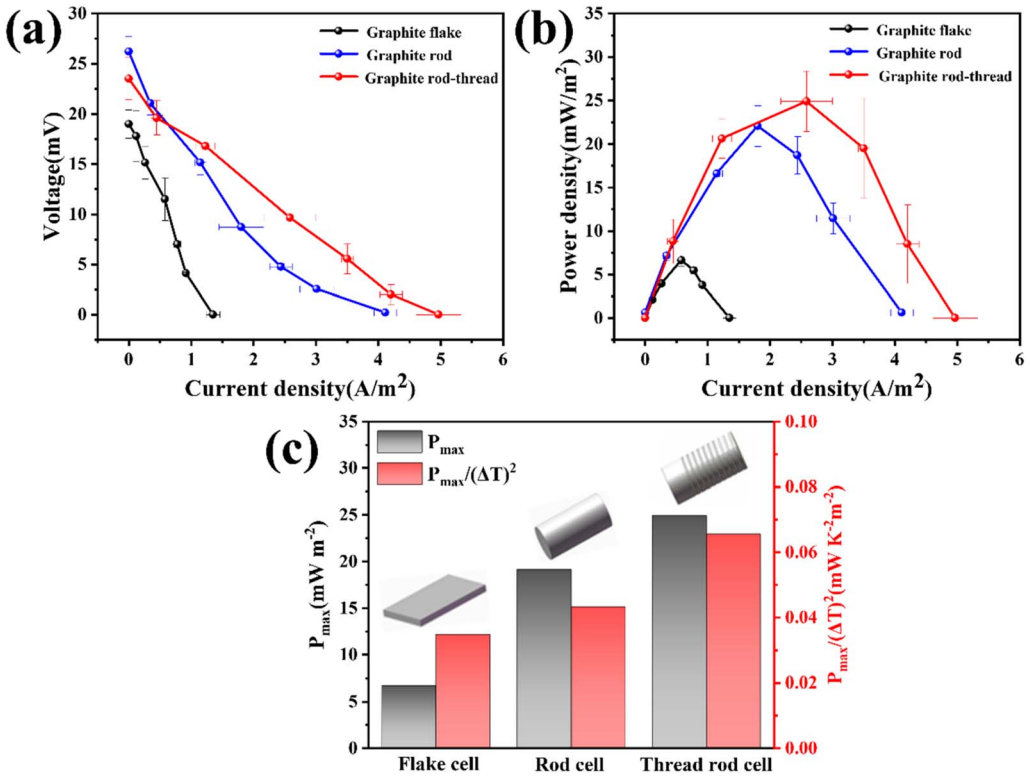

Fig. 3 Thermochemical batteries with different electrode structures: (a) polarization curves, (b) power density curves, and (c) normalized power density ($P_{max}/(\Delta T)^2$).

between the electrode and electrolyte, ensuring effective electrode reaction rates. Meanwhile, the different temperature gradients generated may also enhance ion transport characteristics across the electrode terminals.

3.1.2 Reaction active area test. To investigate why the three-dimensional threaded columnar electrode is more advantageous than the flat-plate electrode structure under the same working conditions, cyclic voltammetry was used to measure the electroactive surface areas provided by the three electrodes. The substrate solution consisted of a 0.05 M Na_2SO_4 and 5 mM $K_4[Fe(CN)_6]$ aqueous solution. As shown in the cyclic voltammograms in Fig. 4, the electrode structure significantly affects the response current. Compared with the two-dimensional flat-plate electrode, the faradaic peak current of the three-dimensional columnar electrode structure increased significantly; the three-dimensional threaded columnar electrode had the highest faradaic peak current. Since all the electrodes used exhibit reversible kinetics, the increase in the faradaic peak current can be attributed to the increase in the electroactive surface area of different electrodes.[25,26] The electroactive surface area can be calculated according to eqn (1):

$$i_p = 0.4664 \times 10^{-3} n F^{3/2} \mathrm{ESA} (RT)^{-1/2} D^{1/2} C v^{1/2} \quad (4)$$

where i_p is the faradaic peak current; n is the number of electrons transferred in the redox reaction; F is the Faraday constant (F = 96 485 C mol^{-1}); R is the gas constant (R = 8.314 J K^{-1} mol^{-1}); T represents the ambient temperature; D is the effective diffusion coefficient; C is the molecular concentration; and v is the scan rate of the voltammetry curve. According to the calculation using eqn (1), the active surface area of the threaded structure increases by 0.6 times compared to the non-threaded columnar electrode, and by 2.1 times compared to the flat-plate electrode structure. This result confirms that the three-dimensional threaded structure exposes more active sites on the electrode, significantly increasing its electroactive surface area and promoting the electron transfer rate of the three-dimensional threaded columnar electrode.

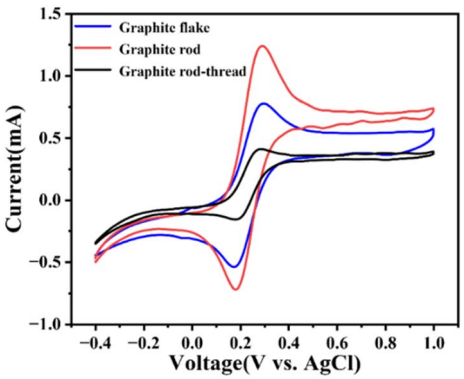

Fig. 4 Cyclic voltammetry scan curves of electrodes with different structures.

3.1.3 Integrated electrode heat dissipation test. In a thermo-electrochemical cell, when a temperature gradient is

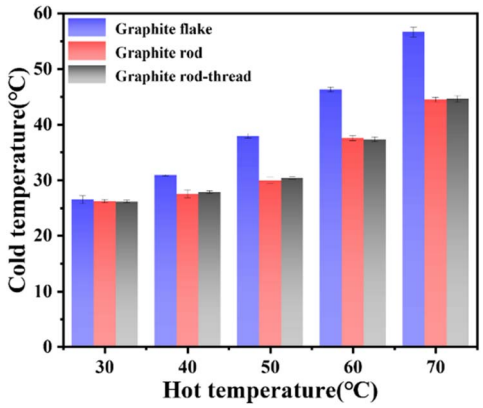

Fig. 5 Cold electrode temperatures of electrodes with different structures at the same hot electrode temperature.

established between two electrodes, the equilibrium of the reversible reaction between redox pairs is disrupted, causing the reactions at the electrodes to incline in opposite directions to generate a potential difference. Under certain conditions, the larger the temperature gradient, the longer this non-equilibrium state persists, the more intense the redox reaction becomes, and the greater the voltage.[27,28] As shown by previous experimental results, the open-circuit voltages of columnar electrodes and threaded rod electrodes are basically the same and significantly higher than those of flat-plate electrodes, so the temperature differences of different electrodes were measured in the experiment. Fig. 5 shows the temperature distribution of the hot and cold electrodes of the three thermo-electrochemical cells. When the hot electrode of the thermo-electrochemical cell remains at the same temperature, the cold electrode temperature of the flat-plate electrode is higher than that of the three-dimensional columnar electrode, and the higher the hot electrode temperature, the more obvious the deviation. For example, when the hot electrode temperature is 30 °C, the cold electrode temperatures of different electrodes are roughly the same, but when the hot electrode temperature rises to 70 °C, the cold electrode temperature of the three-dimensional columnar electrode is significantly 12 °C lower than that of the flat-plate electrode. The results indicate that the three-dimensional columnar electrode has better heat dissipation performance than the flat-plate electrode. Therefore, the three-dimensional columnar electrode increases the temperature difference between the two ends of the thermo-electrochemical cell to a certain extent, generating a larger thermoelectromotive force and improving the output performance of the thermo-electrochemical cell. At the same time, compared with the current traditional cathode heat dissipation of thermo-electrochemical cells, which mainly uses heat sinks added to the cathode surface for heat dissipation, this inevitably increases the thermal resistance between the electrode and the heat sink and complicates the integration of the cathode. The three-dimensional threaded electrode proposed in this paper

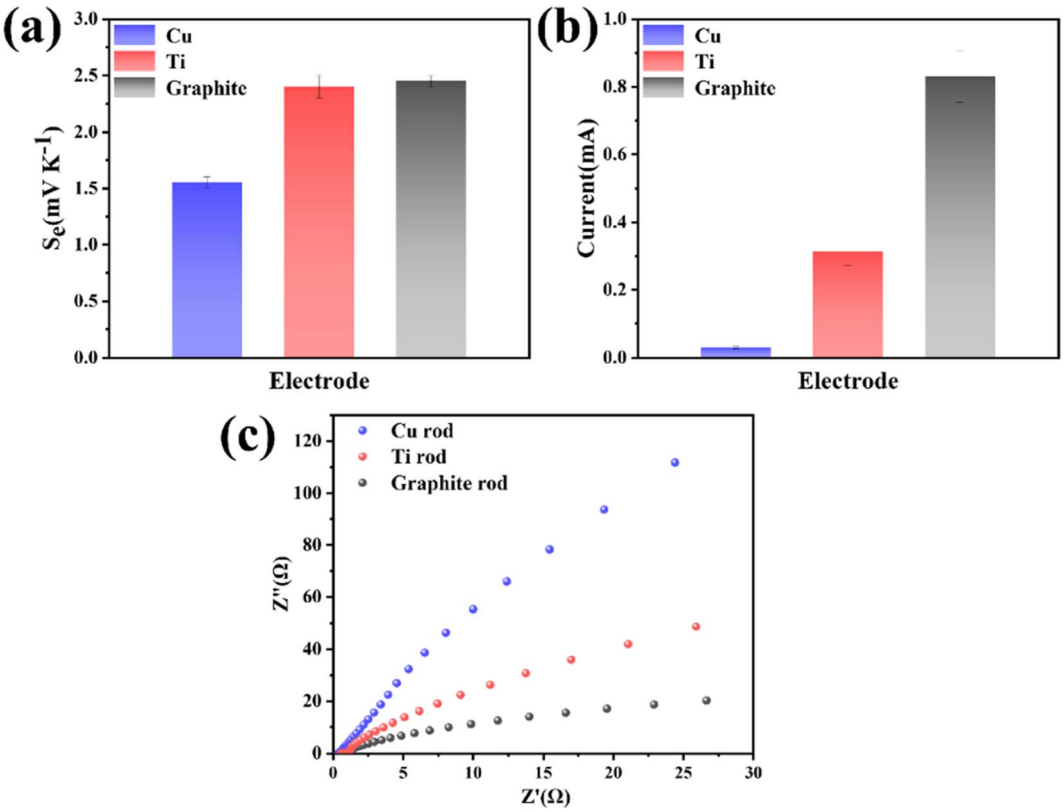

Fig. 6 Thermo-electrochemical cells with different electrode materials: (a) Seebeck coefficient (Se), (b) short-circuit current, and (c) electrochemical impedance spectroscopy tests.

has a significantly larger heat dissipation area (5.04×10^{-4} m^2) than the traditional electrode (1.26×10^{-5} m^2). Meanwhile, the cathode and the heat dissipation part are integrated, which reduces the thermal resistance and provides the possibility for simple integration of electrodes or cell stacks.

3.2 Optimization of the thermo-electrochemical cell system

3.2.1 The influence of electrode materials. A thermo-electrochemical cell is a device that simultaneously undergoes heat exchange and electron transfer. In addition to the same requirements as traditional electrode materials in terms of conductivity, reaction area, and corrosion resistance, its electrode materials also need to have excellent heat conduction capabilities. Platinum electrodes are typical non-reactive catalytic materials that can meet the above requirements, and so early research on thermo-electrochemical cell electrode materials focused on platinum electrodes. However, the high cost of platinum electrode materials significantly increases the output cost. Therefore, it is still necessary to develop thermo-electrochemical cell electrodes with low cost, high electrical and thermal conductivity, and a large surface area.[15,29] As shown in Fig. 6, copper, titanium, and graphite were used as the electrodes of thermo-electrochemical cells to comparatively study the influence of different material electrodes on the performance of thermo-electrochemical cells. Titanium and graphite electrode materials have good stability. To enable copper electrodes to operate stably in the electrolyte of thermo-electrochemical cells, formate solvothermal treatment was applied to modify the surface of copper electrodes, reconstructing the crystals on their surface and forming an ultra-thin surface coordination layer to enhance their stability.

Fig. 6a shows the Seebeck coefficient (Se) of cells with the three electrode materials at the same temperature. The cells with titanium and graphite electrodes showed comparable Seebeck effects, reaching 2.4 mV K^{-1}, while the Se of the copper electrode cell was 1.55 mV K^{-1}. The main reason is that the copper electrode that was thermally treated with formate solution may introduce an ultra-thin modification layer with high oxidation resistance, which limits the redox reaction of the electrolyte and thus restricts the cell voltage and current. The graphite electrode cell has the largest short-circuit current, 2.6 times that of the titanium electrode cell and 28 times that of the copper electrode cell (Fig. 6b). This result can be mainly attributed to two reasons: on the one hand, compared with copper and titanium metal materials, graphite electrodes are usually porous materials and their reaction surface area is significantly larger than that of metal materials, thereby providing a larger active area for reactions;[30,31] on the other hand, the thermal conductivity of titanium electrodes is weaker than that of graphite electrodes.[32,33] Therefore, when the same

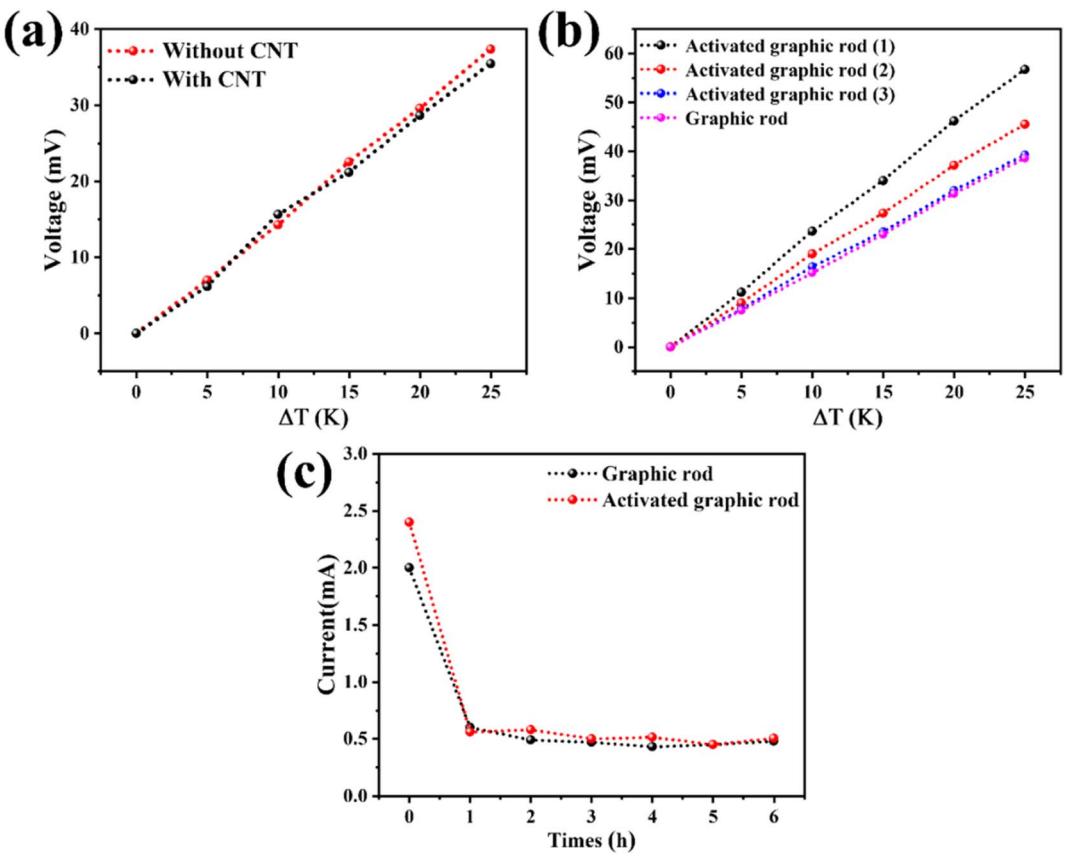

Fig. 7 (a) Seebeck coefficient test of thermo-electrochemical cells with carbon nanotube loading. Testing of thermo-electrochemical cells with NaOH- and high temperature calcination-treated electrodes: (b) Seebeck coefficient and (c) short-circuit output current.

temperature difference is applied, the actual temperature difference between the hot and cold electrodes of the titanium material electrodes is smaller than that of graphite electrodes, resulting in a smaller temperature difference-driven reaction rate at both ends of the electrodes, which leads to the current of the titanium electrodes being significantly smaller than that of graphite electrodes. In addition, as can be seen from the electrochemical impedance spectroscopy tests of the three different electrode materials in Fig. 6c, the graphite electrode exhibited the smallest charge transfer internal resistance at the same applied temperature, further confirming that the graphite electrode surface has the largest temperature difference-driven reaction rate at this time.[34,35]

3.2.2 The influence of electrode surface modification. Electrode materials primarily affect the reaction area and heat exchange process of thermo-electrochemical cells, while surface catalysts or functional groups further influence their catalytic properties. Therefore, the effects of loading catalysts on electrodes or performing pretreatment were investigated to examine their impact on the electrical energy output of thermo-electrochemical cells.[36]

As shown in Fig. 7a, under the same electrode material and reaction temperature difference, traditional carbon nanotube catalysts were loaded onto the electrode surface. At various temperature differences, the loading of catalysts did not significantly affect the output voltage of the thermo-electrochemical cell, with the Seebeck coefficient Se remaining at approximately 1.5 mV K^{-1}. This result may be attributed to the fact that the reaction kinetics of thermo-electrochemical cell electrodes are inherently fast, with a small reaction overpotential, so the catalyst has a limited effect in reducing the overpotential and thus has little impact on the output voltage. Subsequently, the surface of the graphite rod electrode was pretreated with NaOH alkali treatment and high-temperature calcination. As observed in Fig. 7b and c, unlike the catalyst loading, alkali treatment and high-temperature calcination significantly affected the cell's output voltage. This pretreatment increased the cell's output voltage, raising the Seebeck coefficient Se from 1.5 mV K^{-1} to 2.3 mV K^{-1}. However, with repeated use of the electrode, Se gradually decreased and became basically the same as the control sample after multiple uses, while the short-circuit current also matched the control sample. This is because the alkali treatment and high-temperature calcination pretreatment introduced hydroxyl functional groups onto the electrode surface, which interact with ferricyanide to increase the solvation structural entropy of ferricyanide, favoring an increase in Se. However, with repeated use of the electrode, these functional groups are gradually consumed, leading to the disappearance of the enhancement effect.

In summary, due to the fast reaction kinetics of thermo-electrochemical cell electrodes, catalysts have a weak influence on their electrical energy output and are not the main influencing factor. In contrast, the introduction of functional groups affects the structural entropy of the electrolyte. Therefore, future research can focus on altering electrolyte properties to improve the electrical energy output of thermo-electrochemical cells.

3.2.3 The influence of electrode spacing. When external heat is input into a thermo-electrochemical cell, a temperature gradient in the electrolyte is established. Temperature-dependent redox pairs generate a potential difference between the two electrodes at both ends of the electrolyte.[37,38] When heat input is interrupted or weakened, the hot electrode cools ($dT/dt < 0$), and the spontaneous polarization level increases as dipole molecules reorient, leading to a reverse thermoelectric response. Meanwhile, the reduction in the temperature gradient also decreases the thermal response. The temperature gradient between the two electrodes of the cell changes with the electrode spacing, making the control of inter-electrode distance particularly important. In the experiment, a three-dimensional threaded graphite rod was used as the electrode, and the temperature of the hot electrode was maintained at 60 °C to investigate the influence of electrode spacing on the performance of the thermo-electrochemical cell. For a threaded graphite column with an active area A, its thermoelectric current I is expressed as $I = PA dT/dt$, where P is the thermoelectric coefficient and dT/dt is the temperature change rate. As shown in Fig. 8a, the instantaneous current of the cell varies at different spacings and gradually stabilizes as the redox reaction proceeds. With the increase in cell spacing, the transport resistance within the cell increases, the temperature change rate gradually decreases, and the thermoelectric current consequently decreases. Notably, when the distance between the two electrodes is very small, the cell output current is minimized.

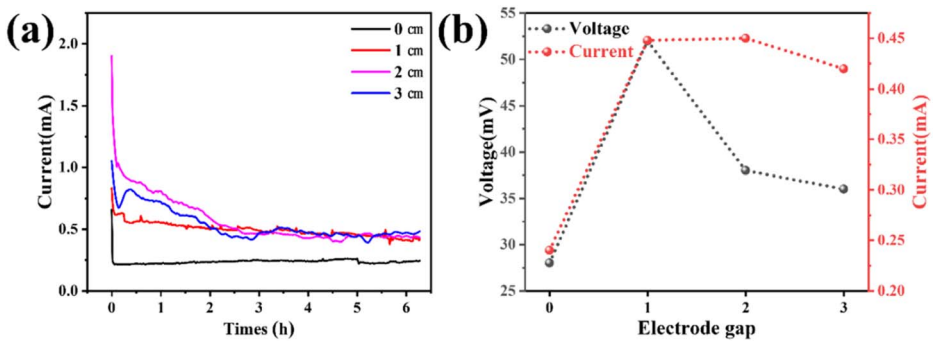

Fig. 8 (a) Current–time curves and (b) voltage–current output values of thermo-electrochemical cells with different electrode spacings.

Fig. 8b shows that the maximum thermal voltage is achieved at an electrode spacing of 1 cm, and the voltage gradually decreases as the spacing increases. This result can be explained as follows: when the electrode spacing is larger, the maximum temperature that the cold electrode can reach is lower, resulting in a larger temperature difference, but the internal resistance also increases. Therefore, in three-dimensional columnar thermo-electrochemical cells, there is a competition between the cell's internal resistance and the temperature gradient for the electrical energy output. When the electrode spacing is small, the temperature difference between the electrodes dominates—smaller temperature differences lead to lower cell voltages, and the output current is also limited by the small temperature difference driving force. When the electrode spacing is relatively large, although a larger temperature difference is beneficial for voltage output, the internal resistance increases with the spacing, causing the open-circuit voltage to peak at 1 cm and then gradually decrease. Therefore, in subsequent experiments, thermo-electrochemical cells were tested with a spacing of 1 cm.

3.2.4 The influence of electrolyte. The Seebeck effect of thermo-electrochemical cells fundamentally originates from the entropy difference of redox electron pairs. The entropy difference of redox pairs is related to their absolute charge, reflecting the interaction strength between redox substances and solvents.[39,40] Ferrocyanide redox pairs are widely studied in thermoelectrochemistry as reaction electrolytes due to their availability, low cost, and high Seebeck coefficient of redox couples.[23,41] However, ferrocyanide redox pairs spontaneously diffuse between the two electrodes in thermo-electrochemical cells, reducing reactant concentration and limiting their Seebeck coefficient. To further increase reactant concentration at both ends of the cell, guanidine hydrochloride (GdmCl) was introduced into the aqueous solution of $[Fe(CN)_6]^{3-}/[Fe(CN)_6]^{4-}$ to improve reactant concentration distribution, and the influence of GdmCl on the performance of thermo-electrochemical cells was investigated. Fig. 9a shows the effect of adding different concentrations of GdmCl on the cell Se value at a fixed temperature difference. As shown, the Se of the thermo-electrochemical cell first increased and then decreased with the increase of GdmCl concentration, reaching a maximum of 2.5 mV K^{-1} at a concentration of approximately 2.0 mol L^{-1}. At this concentration, the Se of the cell was tested by comparing voltage outputs at different temperature differences. As shown in Fig. 9b, within the range of ΔT from 0 to 25 K, the open-circuit voltage is linearly related to the applied temperature difference, and the corresponding Se value calculated from the slope is 2.5 mV K^{-1}, which is a 67% increase compared to the original potassium ferricyanide electrolyte (Se $\approx$ 1.5 mV K^{-1}).

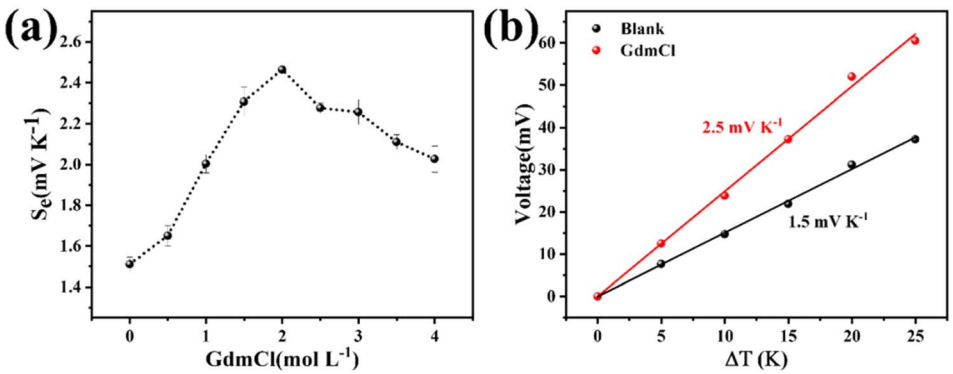

Fig. 9 Thermo-electrochemical cells with different GdmCl concentrations: (a) Seebeck coefficient and (b) voltage output at different temperature differences under the optimal concentration.

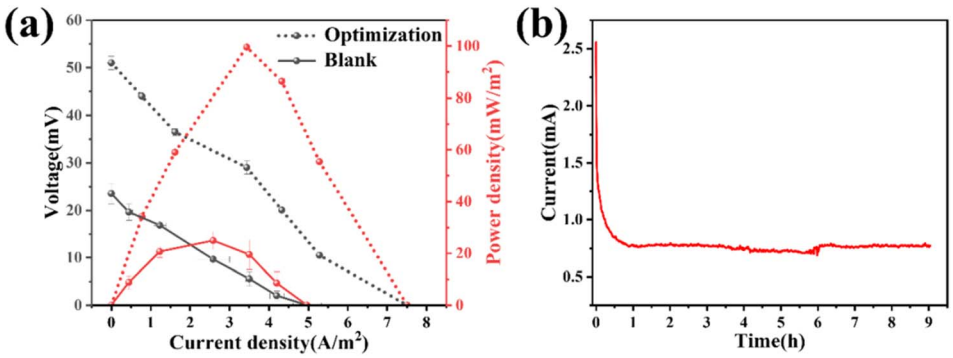

Fig. 10 Power density curve (a) and 9 hour current output curve (b) of the thermo-electrochemical cell with a 1 cm electrode spacing, 2.0 mol per L GdmCl concentration, and catalyst-free threaded graphite electrode.

This result is mainly attributed to the selective induction of $[Fe(CN)_6]^{4-}$ crystallization by guanidine ions (Gdm^+). When Gdm^+ is added to the thermo-electrochemical cell system, $[Fe(CN)_6]^{4-}$ crystallizes on the cold side, then spontaneously precipitates and redissolves on the hot side, increasing the concentration of $[Fe(CN)_6]^{3-}$ near the cold-side electrode and the local concentration of $[Fe(CN)_6]^{4-}$ near the hot-side electrode. This increases the concentration difference entropy caused by reactant concentration around the electrodes, thereby achieving the enhancement of the Seebeck effect driven by both the solvent-dependent entropy difference between redox anions and the concentration difference between the cold and hot sides.

3.3 Optimal performance and stability test of the thermo-electrochemical cell

After optimizing the above parameters, the operating parameters of the thermo-electrochemical cell with optimal performance were obtained. The power generation effect of the optimized thermo-electrochemical cell was tested to evaluate the system's performance. Fig. 10a shows the power output of the thermo-electrochemical cell system under a temperature difference of 20 K. The maximum output power of the optimized cell is 100 mW m^{-2}, which is 3 times higher than the original cell's 25 mW m^{-2}. Meanwhile, its thermal energy conversion efficiency and relative Carnot cycle efficiency reach 0.062% and 1.033%, respectively, which are higher than current

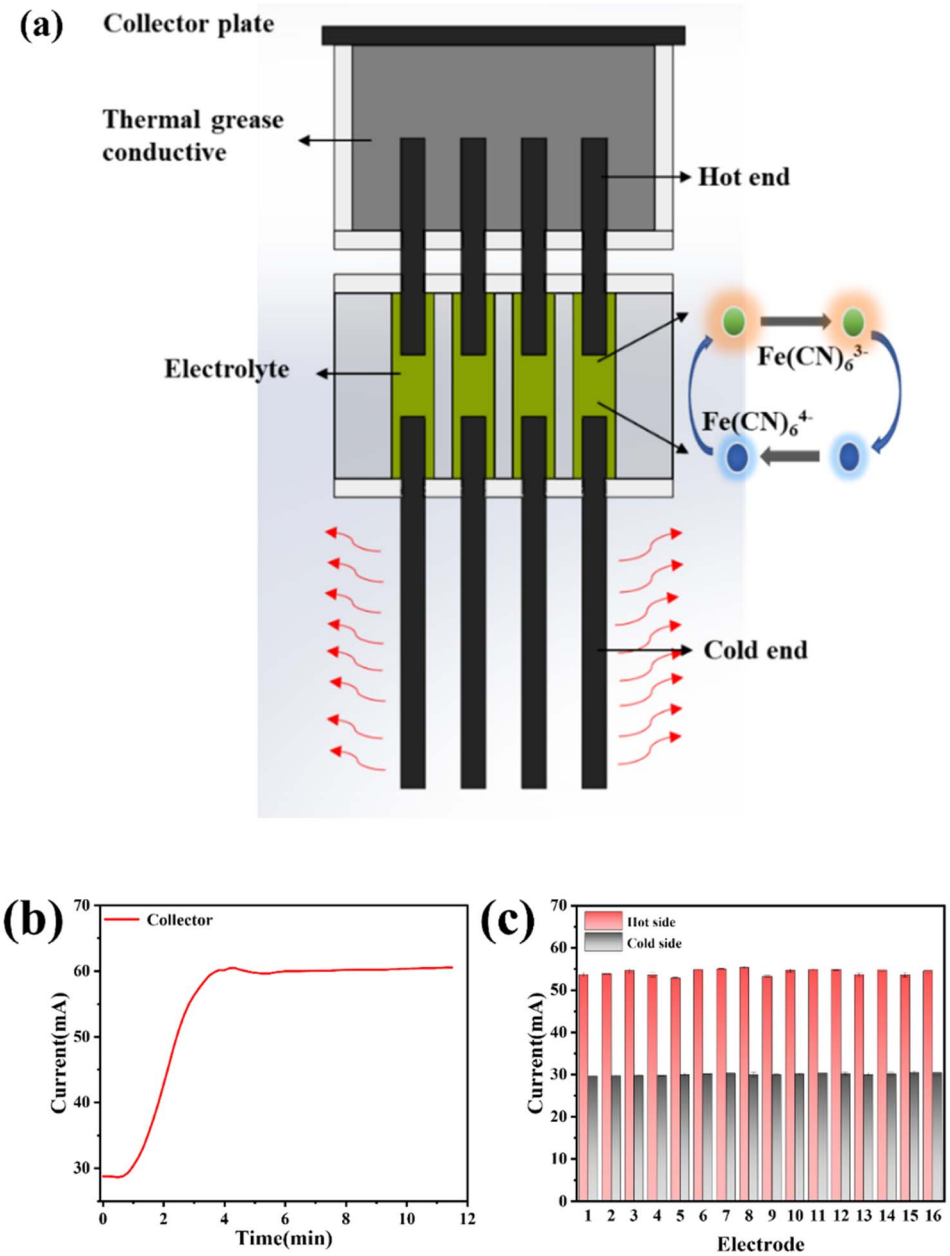

Fig. 11 (a) Schematic of the thermo-electrochemical cell stack structure. (b) and (c) Temperature tests of the hot and cold electrodes.

literature reports.[23,24] In addition, to test the stability of the thermo-electrochemical cell system, the real-time changes in cell current were monitored under stable electrode temperature differences. As shown in Fig. 10b, after 9 hours of monitoring, the cell current remained almost constant at approximately 0.8 mA, indicating that the thermo-electrochemical cell has good stability.

3.4 Integration of thermo-electrochemical cell stacks

Based on the research on single thermo-electrochemical cells, integration from single cells to multiple cells was carried out to obtain higher electrical energy output. A thermo-electrochemical cell stack was prepared, consisting of 16 (4 × 4) independent unit cells connected by copper wires. The stack can switch between series and parallel modes as needed. As shown in Fig. 11, the hot electrodes of the stack are sealed with thermal insulation materials, the chamber is filled with thermal conductive silicone grease, and a graphite plate is used at the bottom as a heat source transmission medium.

To verify the stability and uniformity of heat transfer in the cell stack, as shown in Fig. 11b and c, when the bottom graphite plate is heated to 60 °C by a heat collector, the hot electrode temperature reaches approximately 55 °C, the cold electrode temperature remains at around 30 °C, and the temperature distribution of the 16 electrodes is balanced. This fully demonstrates the feasibility of heat transfer in the cell stack. The specific electrical energy output tests of the stack at different temperatures will be described in the following section.

To explore the series-parallel characteristics of thermo-electrochemical cell stacks, the short-circuit current, open-circuit voltage, and maximum output power of the stack were measured at different temperatures. As shown in Fig. 12a, when the stack is connected in series, a thermal voltage is generated as a temperature difference develops between the hot and cold sides. As the temperature difference across the electrodes gradually increases, the voltage rises. When the hot electrode temperature reaches 80 °C, the maximum open-circuit voltage is approximately 800 mV. Similarly, when the stack is connected

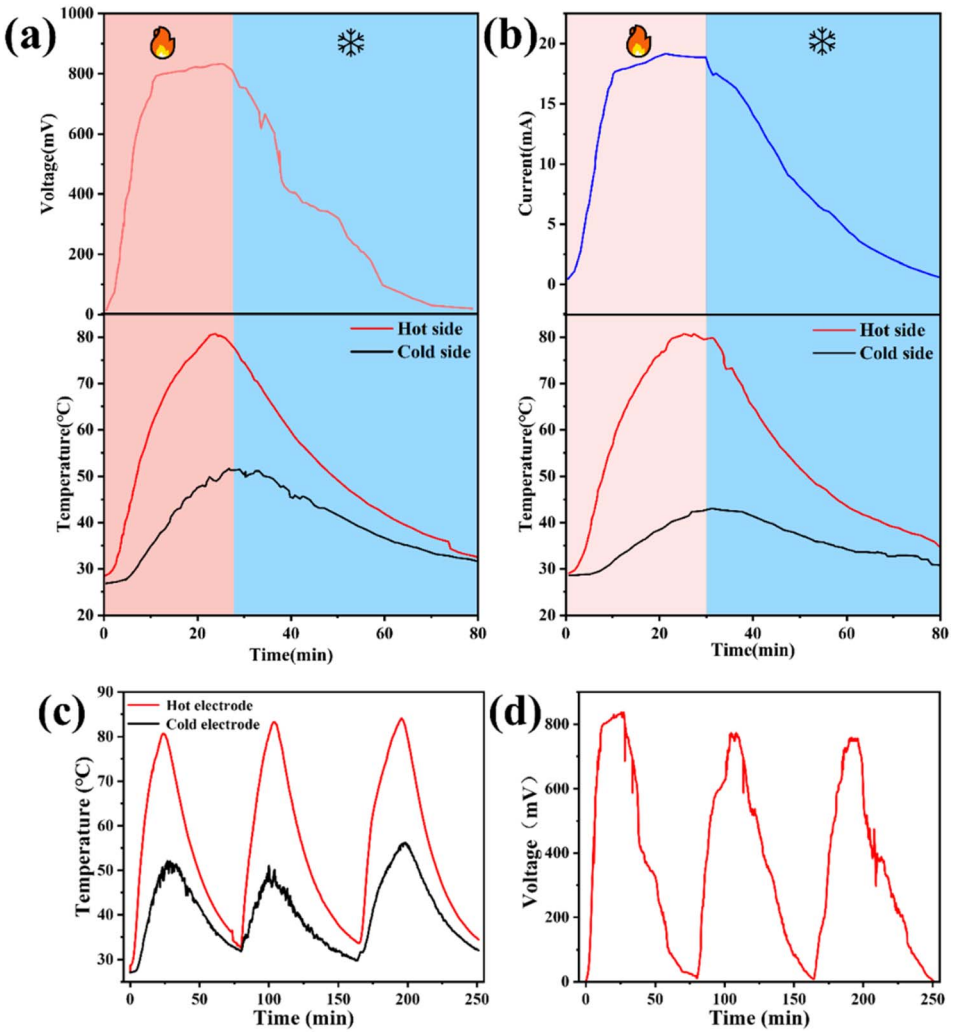

Fig. 12 Voltage–time curves of thermo-electrochemical cell stacks in response to temperature: (a) series connection, (b) parallel connection, and repeatability tests of (c) temperature and (d) voltage for series-connected stacks.

in parallel (Fig. 12b), the short-circuit current reaches 18 mA when the hot electrode temperature reaches 80 °C. When the heat supply from the hot electrode heat collector stops and the temperature difference across the electrodes gradually decreases, the voltage and current are observed to decline immediately, disappearing entirely when no temperature difference remains between the electrodes. Additionally, results from repeated stack experiments (Fig. 12c and d) show good reproducibility between the three electrode heating–cooling curves and the cell voltage curves, further confirming the temperature dependence of thermo-electrochemical cells.

The experiment tested the output power of thermo-electrochemical cell stacks in series and parallel states. As shown in Fig. 13, different hot electrode temperatures significantly affected the output power and voltage of the stacks in both configurations. With increasing temperature, the output voltage of the series-connected stack rose significantly, from 100 mV at 30 °C to approximately 650 mV at 70 °C, while the output power increased from 10 mW to about 240 mW. In the parallel-connected stack, the current increased more prominently, from 3 mA at 30 °C to approximately 17 mA at 70 °C, with output power rising from 24 mW to about 390 mW.

It is evident that the output voltage and current of the stacks are still driven by temperature, and the power output follows the rules of cell series-parallel connections—specifically, the parallel configuration has a smaller total internal resistance and thus higher output power than the series configuration. Since this thermo-electrochemical cell stack can effectively output power in both series and parallel modes, it provides different optional modes for integrating with photoelectrochemical power utilization systems.

3.5 Integration of thermo-electrochemical cell stacks

To further verify the feasibility of thermo-electrochemical cell stacks in practical scenarios, a thermo-electrochemical cell stack composed of 16 independent units (4 × 4 array) in series was constructed based on the optimized single-cell parameters (electrode spacing of 1 cm and electrolyte containing 2.0 mol per L guanidine hydrochloride), and outdoor field tests were carried out. Fig. 14 shows the physical structure, test scenario, and data results of the stack. As shown in Fig. 14c, the stack adopts a modular integrated design: the hot electrode electrodes are sealed with thermal insulation materials to reduce heat loss, the chamber is filled with thermally conductive silicone grease to enhance thermal conduction efficiency, and the bottom graphite plate serves as a heat source-receiving surface to uniformly transfer external heat to each unit cell. This structure not only ensures the stable maintenance of the temperature gradient but also avoids the thermal resistance problem introduced by additional heat sinks through the integrated heat dissipation design of the threaded graphite electrodes, simplifying the system integration complexity.

In the outdoor test (Fig. 14a), the stack was deployed on grassland, using a condenser lens to focus solar energy as the heat source, and a sliding rheostat box to adjust the device angle for optimizing light reception efficiency. The test system was simultaneously connected to a digital multimeter and a thermocouple to collect voltage output and temperature data in real

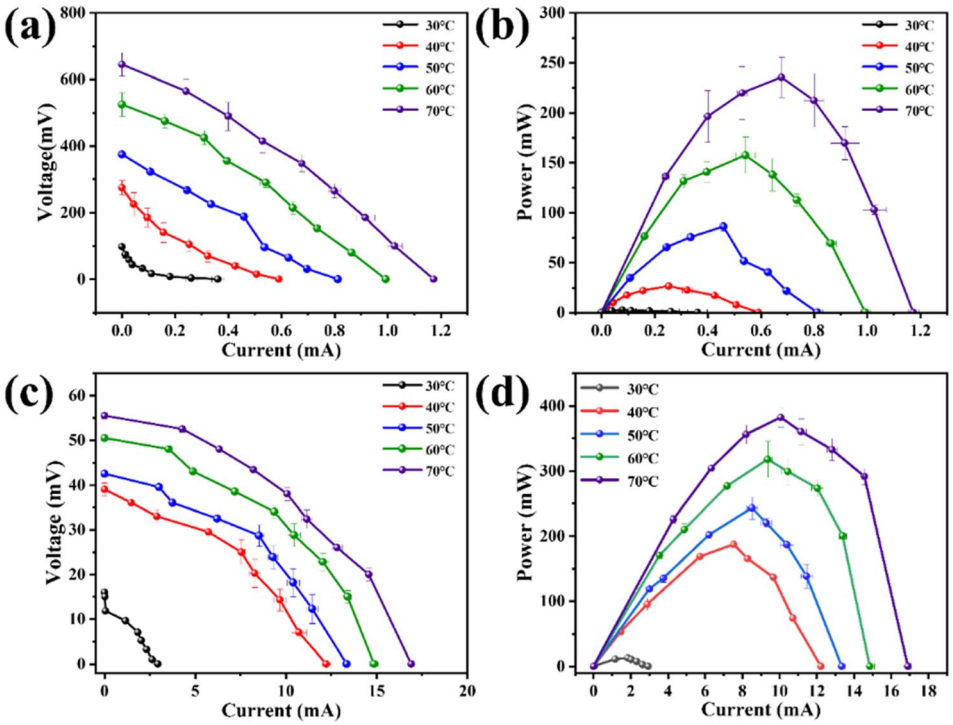

Fig. 13 Polarization curves (a) and power output curves (b) of thermo-electrochemical cell stacks in series connection, and polarization curves (c) and power output curves (d) of stacks in parallel connection.

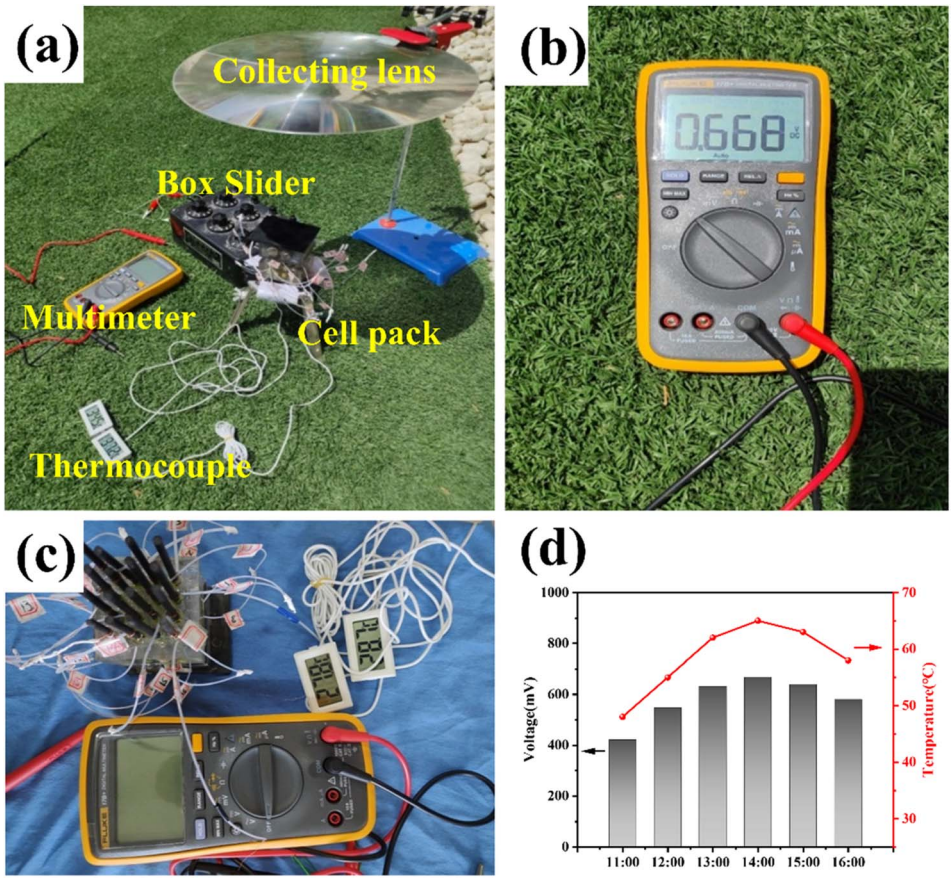

Fig. 14 (a) Outdoor field test diagram of the cell stack. (b) Maximum output voltage. (c) Physical diagram of the cell stack. (d) Field-measured voltage and temperature changes (June 15, 2024, Zhengzhou, Henan).

time. Fig. 14b shows that under typical test conditions, the maximum output voltage of the stack reached 0.668 V, indicating its stable electrical energy conversion capability in natural temperature gradient environments. Fig. 14d records the field-measured data from 11:00 to 16:00 on June 15, 2024, in Zhengzhou, Henan Province. The results show a significant correlation between the voltage output (bar chart) and the ambient temperature (line chart). At around 13:00, when the solar radiation intensity peaked, the hot electrode temperature rose to approximately 65 °C, the cold electrode remained at 30 °C, and the voltage output reached a maximum value of 668 mV; as the sunlight weakened and the temperature difference narrowed, the voltage gradually decreased. The synchronization between voltage fluctuations and temperature changes further verifies the high dependence of thermo-electrochemical cell stacks on temperature gradients and their operational stability.

In summary, the field-measured results in Fig. 14 demonstrate that the threaded graphite electrode thermo-electrochemical cell stack not only exhibits excellent performance under laboratory conditions but can also effectively capture low-grade thermal energy, such as solar energy, in natural environments, providing a highly efficient and practical technical solution for scenarios such as industrial waste heat recovery and distributed energy systems. In the future, optimizing the series-parallel configuration of the stack can further

Table 2 Comparison of reported data and the current work

Electrode	Electrode structure	Se (mV K^{-1})	Power density (mW m^{-2})	Stability (h)	References
Threaded graphite	3D threaded	2.5	100	9	This work
Holey graphene aerogel	Cylinder	1.3	78	—	42
CNT aerogel sheet	Planar and cylindrically wound	1.43	86	—	43
Graphite	Cylindrical disc	1.7	64	0.167	44
Carbon wood	Cubic block	1.5	33	0.1	45
Carbon cloth	2D flat	2.49	16	—	46

improve the system power density and promote its commercialization process.

4 Conclusions

In this study, a thermoelectric cell (TEC) equipped with a threaded graphite electrode was constructed. Experimental results demonstrate that the threaded design of the graphite electrode significantly improves power density owing to a larger electrochemically active surface area (ECSA). Optimization of the TEC, including electrode materials, spacing, and electrolyte composition, enhanced the Seebeck coefficient from 1.5 to 2.5 mV K^{-1}. Based on a single TEC unit, a TEC stack comprising 16 TECs was fabricated, delivering an open-circuit voltage of 0.8 V and a short-circuit current of 18 mA. The feasibility of the TEC stack was further validated under a simulated heat source. The stability and promising power generation performance of the TEC stack highlight its substantial potential for practical applications in low-grade heat recovery. We compared the work done in this paper with previously reported data (Table 2); the comparison highlights the competitive performance and advantages of our threaded graphite electrode design within this field.

Author contributions

Genghua Wang: conceptualization, funding acquisition, formal analysis, resources. Shiwei Zhang: writing-original draft, supervision, formal analysis. Xiaotian Li: conceptualization, visualization, data curation. Jili Zheng: conceptualization, methodology, resources. Lixia Wang: conceptualization, resources, Xinyu Zhou: supervision, Jun Zhang: formal analysis, visualization, writing-review & editing.

Conflicts of interest

The authors declare that they have no known competing financial interests or personal relationships that could have appeared to influence the work reported in this paper.

Data availability

Data will be made available on request.

Acknowledgements

This work was supported by the Science and Technology Department Project of Henan Province (No. 252102220020), Project for the Joint Funds of the Technology Research and Development Program of Henan Province (No. 225200810100), Program for Science & Technology Innovation Talents in Universities of Henan Province (No. 24HASTIT024), the Doctorate Foundation of Zhengzhou University of Light Industry (No. 2025BSJJ052) and Youth Key Teacher Project of Higher Education Institutions in Henan Province (No. 2024GGJS080).

References

1 H. Wang, *et al.*, Thermosensitive-CsI_3^-crystal-driven high-power I^-/I_3^- thermocells, *Cell Rep. Phys. Sci.*, 2022, **3**(3), 100737.
2 M. Rahimi, *et al.*, Emerging electrochemical and membrane-based systems to convert low-grade heat to electricity, *Energy Environ. Sci.*, 2018, **11**(2), 276–285.
3 D. Huo, *et al.*, Progress and prospects for low-grade heat recovery electrochemical technologies, *Sustain. Energy Technol. Assessments*, 2022, **49**, 101802.
4 M. A. Zoui, *et al.*, Design and characterization of a novel finned tubular thermoelectric generator for waste heat recovery, *Energy*, 2022, **253**, 124083.
5 L. O. Freire, *et al.*, Efficiency in thermoelectric generators based on Peltier cells, *Energy Rep.*, 2021, **7**, 355–361.
6 M. Li, *et al.*, High-efficiency thermocells driven by thermo-electrochemical processes, *Trends Chem.*, 2021, **3**(7), 561–574.
7 B. Yu, *et al.*, All-Day Thermogalvanic Cells for Environmental Thermal Energy Harvesting, *Research*, 2019, **2019**, 2460953.
8 S.-M. Jung, *et al.*, Hybrid thermo-electrochemical energy harvesters for conversion of low-grade thermal energy into electricity via tungsten electrodes, *Appl. Energy*, 2021, **299**, 117334.
9 B. Yu, *et al.*, Thermosensitive crystallization-boosted liquid thermocells for low-grade heat harvesting, *Science*, 2020, **370**(6514), 342–346.
10 I. Burmistrov, *et al.*, High seebeck coefficient thermo-electrochemical cell using nickel hollow microspheres electrodes, *Renew. Energy*, 2020, **157**, 1–8.
11 J. Duan, *et al.*, Aqueous thermogalvanic cells with a high Seebeck coefficient for low-grade heat harvest, *Nat. Commun.*, 2018, **9**(1), 5146.
12 H. Ju and J. Kim, Anion-exchanged porous SnTe nanosheets for ultra-low thermal conductivity and high-performance thermoelectrics, *Chem. Eng. J.*, 2020, **402**, 126274.
13 K. Laws, *et al.*, High Seebeck coefficient thermogalvanic cells via the solvent-sensitive charge additivity of cobalt 1,8-diaminosarcophagine, *Chem. Commun.*, 2023, **59**(16), 2323–2326.
14 X. Zhuang, *et al.*, Self-Assembled Asymmetric Electrodes for High-Efficiency Thermogalvanic Cells, *Adv. Energy Mater.*, 2023, **13**(39), 2302011.
15 C.-Y. Lee, S.-H. Hong and C.-L. Liu, Recent Progress in Polymer Gel-Based Ionic Thermoelectric Devices: Materials, Methods, and Perspectives, *Macromol. Rapid Commun.*, 2025, **46**(8), 2400837.
16 X. Qian, *et al.*, Thermodynamics of Ionic Thermoelectrics for Low-Grade Heat Harvesting, *ACS Energy Lett.*, 2024, **9**(2), 679–706.
17 J. Zhang, *et al.*, A novel integrated carbon-wood electrode with photothermal, heat storage, and electrochemical properties for solar-driven thermochemical cells, *Energy Convers. Manage.*, 2025, **326**, 119481.

18 M. Fu, *et al.*, Ionic Thermoelectric Materials Based on the Thermodiffusion Effect: Mechanism, Advancements, and Applications, *Macromol. Chem. Phys.*, 2025, **226**(2), 2400358.
19 Z. Li, *et al.*, Recent progress on the thermoelectric effect for electrochemistry, *J. Mater. Chem. A*, 2024, **12**(23), 13623–13646.
20 H. Im, *et al.*, High-efficiency electrochemical thermal energy harvester using carbon nanotube aerogel sheet electrodes, *Nat. Commun.*, 2016, **7**, 10600.
21 G. Li, *et al.*, High-efficiency cryo-thermocells assembled with anisotropic holey graphene aerogel electrodes and a eutectic redox electrolyte, *Adv. Mater.*, 2019, **31**(25), 1901403.
22 Y. Liu, *et al.*, Potentially Wearable Thermo-Electrochemical Cells for Body Heat Harvesting: From Mechanism, Materials, Strategies to Applications, *Adv. Sci.*, 2021, **8**(13), 2100669.
23 O. Adegoke, *et al.*, Insight into the electrochemical performance of heavy metal-free quantum dots in different buffered ferricyanide/ferrocyanide redox systems, *Mater. Lett.*, 2024, **362**, 136203.
24 W. Qian, *et al.*, Thermo-Electrochemical Cells Based on Carbon Nanotube Electrodes by Electrophoretic Deposition, *Nano-Micro Lett.*, 2016, **8**(3), 240–246.
25 C. S. Movassaghi, *et al.*, Maximizing Electrochemical Information: A Perspective on Background-Inclusive Fast Voltammetry, *Anal. Chem.*, 2024, **96**(16), 6097–6105.
26 B. L. Huffman, A. R. C. Bredar and J. L. Dempsey, Origins of non-ideal behaviour in voltammetric analysis of redox-active monolayers, *Nat. Rev. Chem.*, 2024, **8**(8), 628–643.
27 J. Zhang, *et al.*, Low-Grade Thermal Energy Harvesting and Self-Powered Sensing Based on Thermogalvanic Hydrogels, *Micromachines*, 2023, **14**(1), 155.
28 W. Gao, Y. Wang and F. Lai, Thermoelectric energy harvesting for personalized healthcare, *Smart Med.*, 2022, **1**(1), e20220016.
29 Z. Liu, *et al.*, MXene and Carbon-Based Electrodes of Thermocells for Continuous Thermal Energy Harvest, *Small Methods*, 2023, **7**(8), 2300190.
30 S.-z. Duan, *et al.*, Recent progress in the research and development of natural graphite for use in thermal management, battery electrodes and the nuclear industry, *N. Carbon Mater.*, 2023, **38**(1), 73–95.
31 Z. T. Gossage, *et al.*, New frontiers in alkali metal insertion into carbon electrodes for energy storage, *Chem. Sci.*, 2024, **15**(44), 18272–18294.
32 P.-j. Yang, *et al.*, Progress in the graphitization and applications of modified resin carbons, *N. Carbon Mater.*, 2023, **38**(1), 96–110.
33 J. S. Bulmer, A. Kaniyoor and J. A. Elliott, A Meta-Analysis of Conductive and Strong Carbon Nanotube Materials, *Adv. Mater.*, 2021, **33**(36), 2008432.
34 D. Qu and H.-C. Yu, Multiphysics Electrochemical Impedance Simulations of Complex Multiphase Graphite Electrodes, *ACS Appl. Energy Mater.*, 2023, **6**(6), 3468–3485.
35 B. Zhang, *et al.*, Reliable impedance analysis of Li-ion battery half-cell by standardization on electrochemical impedance spectroscopy (EIS), *J. Chem. Phys.*, 2023, **158**(5), 054202.
36 Z. Liu, *et al.*, Effects of electrode materials, pretreatment, and configuration on gallium electrowinning, *Miner. Eng.*, 2025, **226**, 109248.
37 J. Zhang, *et al.*, Electrochemical reactions in fluidized single-particle catalytic system: from fundamentals to applications, *Chem. Eng. J.*, 2025, **516**, 164248.
38 J. Zheng, *et al.*, Simulation of a thermo-electrochemical cell with graphite rod electrodes, *RSC Adv.*, 2023, **13**(24), 16126–16135.
39 Ø. Gullbrekken, *et al.*, Effect of the Ion, Solvent, and Thermal Interaction Coefficients on Battery Voltage, *J. Am. Chem. Soc.*, 2024, **146**(7), 4592–4604.
40 Y. Guo, *et al.*, Functional Hydrogels for Next-Generation Batteries and Supercapacitors, *Trends Chem.*, 2019, **1**(3), 335–348.
41 M. H. de Sa and C. M. Pereira, The relevance of the initial conditions in glassy carbon electrode sensing applications: the ferri/ferrocyanide redox reaction model system in aqueous solution, *Electrochim. Acta*, 2024, **489**, 144158.
42 G. Qing, *et al.*, Recent Advances and Challenges of Electrocatalytic N_2Reduction to Ammonia, *Chem. Rev.*, 2020, **120**(12), 5437–5516.
43 T. Reier, M. Oezaslan and P. Strasser, Electrocatalytic Oxygen Evolution Reaction (OER) on Ru, Ir, and Pt Catalysts: A Comparative Study of Nanoparticles and Bulk Materials, *ACS Catal.*, 2012, **2**(8), 1765–1772.
44 M. Shen, *et al.*, Quantitative Imaging of Ion Transport through Single Nanopores by High-Resolution Scanning Electrochemical Microscopy, *J. Am. Chem. Soc.*, 2012, **134**(24), 9856–9859.
45 S. Tejedor-Sanz, *et al.*, Geobacter Dominates the Inner Layers of a Stratified Biofilm on a Fluidized Anode During Brewery Wastewater Treatment, *Front. Microbiol.*, 2018, **9**, 378.
46 E. J. E. Stuart, *et al.*, Determining unknown concentrations of nanoparticles: the particle-impact electrochemistry of nickel and silver, *RSC Adv.*, 2012, **2**(17), 6879–6884.